Commun Nonlinear Sci Numer Simulat 98 (2021) 105771

Contents lists available at ScienceDirect

Commun Nonlinear Sci Numer Simulat

journal homepage: www.elsevier.com/locate/cnsns

Research paper

Energy stable discontinuous Galerkin method for compressible Navier–Stokes–Allen–Cahn system

Qiaolin He[a], Xiaoding Shi[b,*]

[a] School of Mathematics, Sichuan University, Chengdu 610064, China
[b] College of Mathematics and Physics, Beijing University of Chemical Technology, Beijing 100029, China

ARTICLE INFO

Article history:
Received 18 July 2020
Revised 2 February 2021
Accepted 14 February 2021
Available online 19 February 2021

Keywords:
Discontinuous Galerkin
Compressible
Navier–Stokes
Allen–Cahn
Two-phase

ABSTRACT

In this paper, we present a fully discrete local discontinuous Galerkin (LDG) finite element method combined with scalar auxiliary variable (SAV) approach for the compressible Navier–Stokes–Allen–Cahn (NSAC) system. We start with a linear and first order scheme for time discretization and the minimal dissipation LDG for spatial discretization, which is based on the SAV approach and is proved to be unconditionally energy stable for one dimensional case. The velocity, the density and the mass concentration of fluid mixture can be solved separately. In addition, a semi-implicit spectral deferred correction (SDC) method combined with the first order scheme is employed to improve the temporal accuracy. Due to the local properties of the LDG methods, the resulting algebraic equations at the implicit level are easy to implement. In particular, we use efficient and practical multigrid solvers to solve the resulting algebraic equations. Although there is no proof of stability for the semi-implicit SDC with LDG spatial discretization, numerical experiments of the accuracy and long time simulations are presented to illustrate the high order accuracy in both time and space, the discretized energy stablity, the capability and efficiency of the proposed method. Numerical results show that the initial state determines the long time behavior of the diffusive interface for the two–phase flow, which are consistent with theoretical asymptotic stability results in Chen et al. (2018)[1].

1. Introduction

Coolant in nuclear power systems is usually operated at high temperature and pressure, therefore, compressible two phase flow is often encountered, for example, the saturated water-vapor systems, etc. A similar phenomenon also occurs in the flow of multipolymers in chemical industries. The motivation for studying this model is to get a better understanding of the nature of these compressible immiscible two-phase flows. In this paper, we are going to introduce a numerical method to study the phase field model for the two phase mixtures of viscous macroscopically immiscible compressible fluid described by the coupled Navier–Stokes–Allen–Cahn system (so called NSAC model). This model was established by Blesgen [2] and was further discussed by Feireisl et al. [3], Heida et al. [4], Chen et al. [1], Ding et al. [5], Kotschote [6] and the

* Corresponding author.
E-mail addresses: qlhejenny@scu.edu.cn (Q. He), shixd@mail.buct.edu.cn (X. Shi).

https://doi.org/10.1016/j.cnsns.2021.105771
1007-5704/

references therein. The compressible Navier–Stokes–Allen–Cahn system is given as follows:

$$\begin{aligned}
&\partial_t \rho + \mathrm{div}(\rho \mathbf{u}) = 0: \quad \text{mass conservation},\\
&\rho \partial_t \mathbf{u} + \rho(\mathbf{u}\cdot\nabla)\mathbf{u} - \mathrm{div}\mathbb{T} = 0: \quad \text{momentum conservation},\\
&\rho \partial_t \chi + \rho \mathbf{u}\nabla\chi = -\mu: \quad \text{the motion of the interfaces between immiscible fluids},\\
&\rho\mu = \frac{\rho}{\epsilon}\frac{\partial f}{\partial \chi} - \epsilon\Delta\chi: \quad \text{the definition of the chemical potential},
\end{aligned} \tag{1}$$

which describes the evolution of the binary compressible mixture, where the unknown functions ρ, $\mathbf{u}$, χ and μ denote the total density, the mean velocity, the mass concentration of fluid mixture (phase field variable) and the chemical potential, respectively, where $f = f(\chi)$ is the potential free energy density which can have different formulas in different problems and $\mathbb{T}$ is the Cauchy stress–tensor

$$\mathbb{T} = \nu\nabla\mathbf{u} + \lambda \mathrm{div}\mathbf{u}\mathbb{I} - p(\rho)\mathbb{I} - \epsilon\nabla\chi\otimes\nabla\chi + \frac{\epsilon}{2}|\nabla\chi|^2\mathbb{I}, \tag{2}$$

here $\mathbb{I}$ is the unit matrix, $\nu > 0$, $\lambda > 0$ are viscosity coefficients, $\epsilon > 0$ is the thickness of the diffuse interface of the fluid mixture and $p = p(\rho)$ is the pressure. The compressible NSAC system has been applied to such applications as vesicle membranes, complex fluids like liquid crystals with non-conserved order parameters, and fluid mixtures with phase transitions or chemical reactions where the volume fraction of each component are not necessarily conserved. In numerical scheme and stability analysis, we focus on the one dimensional NSAC system, which is as follows:

$$\rho_t + (\rho u)_x = 0, \tag{3a}$$

$$\rho u_t + \rho u u_x + p_x = \nu u_{xx} - \frac{\epsilon}{2}\left(\chi_x^2\right)_x, \tag{3b}$$

$$\rho\chi_t + \rho u\chi_x = -\frac{1}{\epsilon}f_\chi + \frac{\epsilon}{\rho}\chi_{xx}, \tag{3c}$$

where $x \in (a, b)$ and $t > 0$, with the initial boundary condition

$$(\rho, u, \chi)(x, 0) = (\rho_0, u_0, \chi_0)(x), \ \ x \in (a, b), \tag{4}$$

and the periodic boundary condition or the homogeneous Neumann boundary condition. All the physical quantities in the above equations are dimensionless. Next we will discuss the formulation of the pressure $p(\rho)$.

In dealing with the behavior of a fluid near liquid-vapor phase transition, the equation of state proposed by van der Waals is quite satisfactory in many aspects, which commonly expressed as

$$\left(p + \frac{C_1}{V^2}\right)(V - C_2) = R\Theta, \tag{5}$$

where p is pressure, V is volume, Θ is temperature, R is the gas constant, and C_1 and C_2 are constants characterizing the effect of the molecular cohesive forces and the finite size of the molecules. After dimensionless calculation [7], Eq. (5) becomes

$$\left(p + \frac{3}{V^2}\right)\left(V - \frac{1}{3}\right) = \frac{8}{3}\Theta, \tag{6}$$

where p, V and Θ are corresponding dimensionless physical quantities. The pressure can be written as

$$p = -3\rho^2 + \frac{8\Theta\rho}{3 - \rho}, \tag{7}$$

where $\rho = \frac{1}{V}$ is the density. For $\Theta < 1$, there is an interval of ρ where p increases as ρ decreases, see [7,8]. Phase transition takes place around the region where $p(\rho)$ is increasing. There are a lot of numerical studies concerning the conservation law without phase variable, see [9–11]. In [12,13], the authors study the van der Waals system in the Eulerian coordinates. They have shown that how phase transition takes place and what is the long time behavior of such system. If the initial data belongs to elliptic region, the solution converges to two Maxwell states. When the initial data lies in metastable region, the solution either remains in the same phase or converges to the Maxwell states depending on the initial perturbation. If the initial state is in the stable region, the solution remains in that region for all time.

There are some works about incompressible Navier–Stokes–Cahn–Hilliard (NSCH) system which is used to model the evolution of the binary incompressible mixture, see [14,15]. In [16], an accurate and energy stable discontinuous Galerkin method has been presented for phase field models of two–phase incompressible flow. There are also other related works about incompressible system. But as far as we know, for quasi–incompressible and compressible models, there are few works. We use a relaxation scheme coupled with a stabilized method to numerically study the compressible NSCH system, which has energy decaying property under certain conditions with $p = \rho^\gamma$, see [17].

In order to study phase transition and long time behavior in van der Waals fluid, we are going to simulate the compressible NSAC system. There are several components in our numerical method. Shen et al. [18] introduced a scalar auxiliary

variable (SAV) to solve various gradient flows, which is independent of the space variable and is bounded from below. The SAV approach leads to a numerical scheme that is unconditionally energy stable and easy to implement. In our work, this approach is used in the equation of the chemical potential. Regarding spatial discretization, we will pay particular attention to the local discontinuous Galerkin (LDG) method, which is to suitably rewrite a higher order PDE [19] into a first order system, then apply the discontinuous Galerkin (DG) method to the system. The first LDG method was developed by Cockburn and Shu [20] to solve the convection diffusion equation containing second derivatives. The authors [21] presented the first a priori error analysis for the LDG method for a model elliptic problem. Cockburn and Dong [22] analyzed the minimal dissipation LDG method and showed that it has the same convergence properties as all other known DG methods even though its stabilization parameters are identically equal to zero in the interior of the domain. More recently, the LDG methods have been further successfully used to simulate many phase field models, including the Cahn–Hilliard equation [23], the Cahn–Hilliard–Hele–Shaw system [24], the Cahn–Hilliard–Brinkman system [25], the functionalized Cahn–Hilliard equation [26] and the phase field crystal equation [27]. A key ingredient for the success of such methods is the correct design of interface numerical fluxes. These fluxes must be designed to guarantee stability and local solvability of all the auxiliary variables introduced to approximate the derivatives of the solution. The LDG method can retain the flexibility of the DG method since the auxiliary variables can be locally eliminated. All of these good properties motivate us to develop the LDG method for the NSAC system. Spectral deferred correction (SDC) [28] method was proposed for ODEs and can achieve arbitrary order accuracy in time. The SDC begins by converting the original ODEs into the corresponding Picard equation and apply a deferred correction procedure in the integral formulation, driven by either the explicit or the implicit Euler marching scheme. In [29], the authors developed a semi-implicit SDC method to solve a series of highly nonlinear time dependent PDEs, which can improve the temporal accuracy.

We develop a decoupled scheme, which is first order in time discretization and is energy stable. The χ, ρ, $\mathbf{u}$ can be solved separately, therefore the scheme is efficient to implement. The semi-implicit SDC method combined with the first order scheme is employed to improve the temporal accuracy and the local truncation error of the SDC [29] is $O(\tau^{\min[K+1,P+1]})$ with $\tau = \max_{n,m} \Delta t_{n,m}$, where time interval $[t_n, t_{n+1}]$ is divided into P subintervals and $\Delta t_{n,m}$ is the length of a subinterval, and K is the number of the successive corrections in SDC. Due to the local properties of the LDG method, the resulting algebraic equations at the implicit level are easy to implement. Specially, when the problem is linear, a linear solver is involved in the resulting algebraic equations and we perform a LU decomposition at the beginning and use it for all time steps when using a fixed time step. But for NSAC system which is nonlinear and coupled, we use multigrid solver in each time step for efficiency.

The rest of this article is organized as follows. In Section 2, the energy law for the NSAC system (3a)–(3c) is described. In Section 3, we propose a LDG scheme combined with SAV method which is linear and decoupled, and prove the unconditional energy stability of fully–discrete scheme for one dimensional case. The semi-implicit SDC method is employed to achieve high order temporal and spatial accuracy. Numerical experiments are presented in Section 4, demonstrating the accuracy and efficiency of the proposed numerical method. The paper concludes in Section 5 with some remarks.

2. Energy law for the system

In this section, we will present the energy equation of system (3a)–(3c). The function $G(\rho)$ is defined by (8), which was introduced in Blesgen [2] and Feireis et al. [3].

$$\rho^2 G'(\rho) = p(\rho), \text{ or, equivalently, } G(\rho) = \int_{0.3}^{\rho} \frac{p(z)}{z^2} dz, \tag{8}$$

where

$$p = p(\rho) \in C^1(0, \infty), \tag{9}$$

is assumed to be a known function of the density. The function $G(\rho)$ is used to penalize the density changes for large values of the pressure. Here the value 0.3 is in stable region for temperature $\Theta = 0.9$ in van der Waals fluid, this value can be replaced by any other values in stable region. Since $\rho = 1/V$, it is easy to observe that $G(\rho)$ is a integration of pressure $p(V)$, which is the work done by pressure due to the variation of volume. Combined with the mass conservation equation (3a), we obtain that

$$\big(\rho G(\rho)\big)_t + \big(\rho u G(\rho)\big)_x + \big(p(\rho)\big)u_x = 0. \tag{10}$$

The following lemma shows that the kinetic energy, the work done by pressure and the free energy at the interface are uniformly bounded with respect to time.

Lemma 2.1. *Let $I = (a, b)$, assuming that $\rho_0, u_0 \in H^1(I)$; $\chi_0 \in H^2(I)$; and both periodic and zero Neumann boundary conditions for ρ, u and χ, then for $T > 0$ it holds that*

$$\begin{aligned} &\sup_{t\in[0,T]} \int_I \left(\frac{\rho u^2}{2} + \frac{\epsilon}{2}|\chi_x|^2 + \rho G(\rho) + \frac{\rho f(\chi)}{\epsilon} \right) dx + \int_0^T \int_I \Big(|\mu|^2 + \nu |u_x|^2 \Big) dx dt \\ &\le \int_I \left(\frac{1}{2}\rho_0 u_0^2 + \frac{\epsilon}{2}|\chi_{0x}|^2 + \rho_0 G(\rho_0) + \frac{\rho_0 f(\chi_0)}{\epsilon} \right) dx, \end{aligned} \tag{11}$$

where $\mu = \frac{1}{\epsilon}\frac{\partial f}{\partial \chi} - \frac{\epsilon}{\rho}\chi_{xx}$ *is the chemical potential.*

Proof. In order to get the energy inequality (11), we use the usual energy estimation method. The idea of this method is to obtain various energy estimates by multiplying the conservation of mass equation, momentum equation and phase field equation by the function of density, velocity and chemical potential respectively. The process is as follows:

Multiplying Eq. (3b) by u and Eq. (3c) by μ, integrating over I and adding them up, using the boundary conditions, one has

$$\frac{d}{dt}\int_I \Big(\frac{\rho u^2}{2} + \frac{\epsilon}{2}|\chi_x|^2 + \frac{\rho f(\chi)}{\epsilon}\Big)dx + \int_I \Big(|\mu|^2 + \nu|u_x|^2 + up_x\Big)dx = 0.$$

Integrating (10) and adding the result to the above equation, one then gets

$$\frac{d}{dt}\int_I \Big(\frac{\rho u^2}{2} + \frac{\epsilon}{2}|\chi_x|^2 + \rho G(\rho) + \frac{\rho f(\chi)}{\epsilon}\Big)dx + \int_I \Big(|\mu|^2 + \nu|u_x|^2\Big)dx = 0,$$

integrating the above equation over $[0, T]$, one has

$$\sup_{t\in[0,T]}\int_I \Big(\frac{\rho u^2}{2} + \frac{\epsilon}{2}|\chi_x|^2 + \rho G(\rho) + \frac{\rho f(\chi)}{\epsilon}\Big)dx + \int_0^T\int_I \Big(|\mu|^2 + \nu|u_x|^2\Big)dxdt$$

$$\le \int_I \Big(\frac{1}{2}\rho_0 u_0^2 + \frac{\epsilon}{2}|\chi_{0x}|^2 + \rho_0 G(\rho_0) + \frac{\rho_0 f(\chi_0)}{\epsilon}\Big)dx, \tag{12}$$

the standard energy estimate (11) is obtained. □

Remark 2.1. Although the Lemma 2.1 is for one dimensional case, it can be easily extended to arbitrary dimensional case.

3. A LDG method combined with SAV

Next, we will develop a linear and decoupled scheme, using the SAV approach [18], which by introducing a scalar auxiliary variable to design unconditionally, first- and second-order energy-stable schemes for a large class of gradient flows. The auxiliary variable is a function of the integration of free energy density in NSAC system and only depends on time. This SAV approach only requires the nonlinear energy functional be bounded from below. In order to develop the linear scheme, we briefly describe the SAV approach. We define $E_1(\chi) := \int_I \rho f(\chi)dx$, $I = (a, b)$, where $f(\chi) = \frac{1}{4}(\chi^2 - 1)^2$, the double well potential which is used to describe the interface between two phase flow. Usually, $E_1(\chi) \ge -C_0$, which means E_1 is bounded below. In our problem, it is observed that $E_1(\chi) \ge 0$. We introduced an auxiliary function as follows

$$r(t) = \sqrt{E_1(\chi)},$$

which only depends on time variable t. Then (3a)–(3c) can be rewritten as:

$$\begin{aligned}
&\rho u_t + \rho u u_x + p_x = \nu u_{xx} - \frac{\epsilon}{2}\big(\chi_x^2\big)_x,\\
&\rho\chi_t + \rho u\chi_x = -\mu,\\
&\mu = \frac{1}{\epsilon}\frac{r(t)}{\sqrt{E_1(\chi)}}f_\chi - \frac{\epsilon}{\rho}\chi_{xx},\\
&r_t = \frac{1}{2\sqrt{E_1(\chi)}}\int_I(\rho f_\chi\chi_t + \rho_t f)dx\\
&\rho_t + (\rho u)_x = 0,
\end{aligned} \tag{13}$$

3.1. The semi-discrete scheme in time using SAV

For (13), we now construct a semi-implicit linear and first order scheme in time discretization.

$$\begin{aligned}
&\rho^n\frac{u^* - u^n}{\Delta t} + p_x^n = -\epsilon\chi_x^n\chi_{xx}^{n+1},\\
&\rho^n\frac{\chi^{n+1} - \chi^n}{\Delta t} + \rho^n u^*\chi_x^n = -\mu^{n+1},\\
&\mu^{n+1} = \frac{r^{n+1} + r^n}{2\epsilon\sqrt{E_1(\chi^n)}}f_\chi^n - \frac{\epsilon}{\rho^n}\chi_{xx}^{n+1},\\
&\frac{r^{n+1} - r^n}{\Delta t} = \frac{1}{2\sqrt{E_1(\chi^n)}}\int_I\Big(\rho^n f_\chi^n\frac{\chi^{n+1} - \chi^n}{\Delta t} + \frac{\rho^{n+1} - \rho^n}{\Delta t}f^n\Big)dx,
\end{aligned}$$

$$\frac{\rho^{n+1}-\rho^n}{\Delta t}+(\rho^n u^*)_x=0,$$
$$\rho^n\frac{u^{n+1}-u^*}{\Delta t}+\rho^n u^* u_x^{n+1}=\nu u_{xx}^{n+1}. \tag{14}$$

3.2. Implementation details

We can eliminate μ^{n+1} and r^{n+1} from (14) to obtain that

$$\begin{aligned}&\left(\frac{\rho^n}{\Delta t}-\left(\frac{\epsilon}{\rho^n}+\epsilon\Delta t(\chi_x^n)^2\right)\partial_{xx}\right)\chi^{n+1}+\frac{f_\chi^n}{4\epsilon E_1(\chi^n)}\left(\rho^n f_\chi^n,\chi^{n+1}\right)-\frac{(\Delta t)^2 f_\chi^n}{4E_1(\chi^n)}\left(\chi_x^n f_x^n,\chi_{xx}^{n+1}\right)\\&=\frac{\rho^n}{\Delta t}\chi^{n+1}-\left(\frac{\epsilon}{\rho^n}+\epsilon\Delta t(\chi_x^n)^2\right)\chi_{xx}^{n+1}+\frac{f_\chi^n}{4E_1(\chi^n)}\left(\frac{1}{\epsilon}\rho^n f_\chi^n-(\Delta t)^2(\chi_x^n f_x^n)_{xx},\chi^{n+1}\right)\\&=g^n,\end{aligned} \tag{15}$$

where $(\cdot,\cdot)$ is the L^2 integral in I, the right–hand side term is defined as

$$g^n=\frac{\rho^n\chi^n}{\Delta t}-(\rho^n u^n-\Delta t p_x^n)\chi_x^n-\frac{r^n f_\chi^n}{\epsilon\sqrt{E_1(\chi^n)}}+\frac{f_\chi^n}{4\epsilon E_1(\chi^n)}\left(\rho^n f_\chi^n,\chi^n\right)-\frac{\Delta t f_\chi^n}{4\epsilon E_1(\chi^n)}(\rho^n u^n-\Delta t p_x^n,f_x^n), \tag{16}$$

and periodic boundary condition is used. Let $b^n=\frac{1}{\epsilon}\rho^n f_\chi^n-(\Delta t)^2(\chi_x^n f_x^n)_{xx}$ and $A=\frac{\rho^n}{\Delta t}E-\left(\frac{\epsilon}{\rho^n}+\epsilon\Delta t(\chi_x^n)^2\right)\partial_{xx}$, where E is the identity operator, then (15) can be written as

$$A\chi^{n+1}+\frac{f_\chi^n}{4E_1(\chi^n)}\left(b^n,\chi^{n+1}\right)=g^n. \tag{17}$$

Multiplying (17) with A^{-1}, then taking the inner product with b^n, we obtain

$$(b^n,\chi^{n+1})+\frac{1}{4E_1(\chi^n)}(A^{-1}f_\chi^n,b^n)(b^n,\chi^{n+1})=(b^n,A^{-1}g^n). \tag{18}$$

Therefore, we have

$$(b^n,\chi^{n+1})=\frac{(b^n,A^{-1}g^n)}{1+\frac{1}{4E_1(\chi^n)}(A^{-1}f_\chi^n,b^n)}. \tag{19}$$

From (17), χ^{n+1} is solved by

$$\chi^{n+1}=-\frac{(b^n,A^{-1}g^n)}{1+\frac{1}{4E_1(\chi^n)}(A^{-1}f_\chi^n,b^n)}A^{-1}\frac{f_\chi^n}{4E_1(\chi^n)}+A^{-1}g^n. \tag{20}$$

Hence, the total cost for solving χ^{n+1} at each time step are essentially solving two second order differential equations with variable coefficients. The computation of phase variable χ is decoupled with that of velocity u and density ρ. In addition, the use of u^* eliminates the tight coupling relationship between χ and u. Hence, the scheme makes less computations and is more efficient compared to the coupled system.

3.3. Fully–discrete scheme and its stability

In this section, we will develop the fully–discrete LDG method for the proposed scheme (14). The LDG method is an extension of the DG method aimed at solving PDEs containing higher order spatial derivatives. The DG method is a class of finite element methods using completely discontinuous basis functions, to approximate the discrete solutions. There are usually two steps to implement the LDG method: first rewriting the problem into a form which contains only first order derivatives, and then applying the DG method by choosing appropriate numerical fluxes to ensure stability. So we introduce two variables $w^{n+1}=\chi_x^{n+1}$ and $q^{n+1}=u_x^{n+1}$. Let $I_j=[x_{j-\frac{1}{2}},x_{j+\frac{1}{2}}]$, for $j=1,\dots,J$, be a subdivision of I. Associated with this mesh, we define the discontinuous Galerkin finite element spaces

$$W_h=\{v:v\in\mathcal{P}^k(I_j)\quad\text{for}\quad x\in I_j,j=1,\dots,J\},$$

where $\mathcal{P}^k(I_j)$ denotes the space of polynomials of degree at most $k\geq 0$ on I_j. We denote by $(u_h^{n+})_{j+\frac{1}{2}}$ and $(u_h^{n-})_{j+\frac{1}{2}}$ the values of u_h^n at $x_{j+\frac{1}{2}}$, from the right cell I_{j+1}, and from the left cell I_j, respectively.

Firstly we rewrite (14) into the system form

$$\begin{aligned}
&\rho^n \frac{u^* - u^n}{\Delta t} + p_x^n = -\epsilon w^n w_x^{n+1},\\
&\rho^n \frac{\chi^{n+1} - \chi^n}{\Delta t} + \rho^n u^* \frac{\partial \chi^n}{\partial x} = -\mu^{n+1},\\
&\mu^{n+1} = \frac{r^{n+1} + r^n}{2\epsilon\sqrt{E_1(\chi^n)}} f_\chi^n - \frac{\epsilon}{\rho^n} w_x^{n+1},\\
&\frac{r^{n+1} - r^n}{\Delta t} = \frac{1}{2\sqrt{E_1(\chi^n)}} \int_I \left(\rho^n f_\chi^n \frac{\chi^{n+1} - \chi^n}{\Delta t} - (\rho^n u^*)_x f^n \right) dx,\\
&\frac{\rho^{n+1} - \rho^n}{\Delta t} + (\rho^n u^*)_x = 0,\\
&\rho^n \frac{u^{n+1} - u^*}{\Delta t} + \rho^n u^* \frac{\partial u^{n+1}}{\partial x} = \nu q_x^{n+1},\\
&w^{n+1} = \chi_x^{n+1},\\
&q^{n+1} = u_x^{n+1},
\end{aligned} \tag{21}$$

which contains only first order spatial derivatives. Then we apply the discontinuous Galerkin method to solve (21), resulting in the following LDG scheme: Find $u^*,\ \chi_h^{n+1},\ \mu_h^{n+1},\ \rho_h^{n+1},\ u_h^{n+1},\ w_h^{n+1},\ q_h^{n+1} \in W_h$, such that, $\forall\ \eta_1,\ \eta_2,\ \eta_3,\ \eta_4,\ \eta_5,\ \eta_6,\ \eta_7 \in W_h$, we have

$$\int_{I_j} \rho_h^n \frac{u^* - u_h^n}{\Delta t} \eta_1 dx - \int_{I_j} p_h^n \eta_{1x} dx + (\widehat{p}_h^n \eta_1^-)_{j+\frac{1}{2}} - (\widehat{p}_h^n \eta_1^+)_{j-\frac{1}{2}} = -\epsilon \int_{I_j} \frac{\partial w_h^{n+1}}{\partial x} w_h^n \eta_1 dx \tag{22}$$

$$\int_{I_j} \rho_h^n \frac{\chi_h^{n+1} - \chi_h^n}{\Delta t} \eta_2 dx + \int_{I_j} \rho_h^n u^* \frac{\partial \chi_h^n}{\partial x} \eta_2 dx = -\int_{I_j} \mu_h^{n+1} \eta_2 dx, \tag{23}$$

$$\int_{I_j} \rho_h^n \mu_h^{n+1} \eta_3 dx = \frac{r^{n+1} + r^n}{2\epsilon\sqrt{E_1(\chi_h^n)}} \int_{I_j} \rho_h^n \frac{\partial f^n}{\partial \chi_h^n} \eta_3 dx + \int_{I_j} \epsilon w_h^{n+1} \eta_{3x} dx - \epsilon(\hat{w}_h^{n+1} \eta_3^-)_{j+\frac{1}{2}} + \epsilon(\hat{w}_h^{n+1} \eta_3^+)_{j-\frac{1}{2}}, \tag{24}$$

$$\frac{r^{n+1} - r^n}{\Delta t} = \frac{1}{2\sqrt{E_1(\chi^n)}} \int_\Omega \left(\rho_h^n \frac{\partial f^n}{\partial \chi_h^n} \frac{\chi_h^{n+1} - \chi_h^n}{\Delta t} - (\rho_h^n u^*)_x f^n \right) dx \tag{25}$$

$$\int_{I_j} \frac{\rho_h^{n+1} - \rho_h^n}{\Delta t} \eta_4 dx - \int_{I_j} \rho_h^n u^* \eta_{4x} dx + (\widehat{\rho_h^n u^*} \eta_4^-)_{j+\frac{1}{2}} - (\widehat{\rho_h^n u^*} \eta_4^+)_{j-\frac{1}{2}} = 0, \tag{26}$$

$$\int_{I_j} \rho_h^n \frac{u_h^{n+1} - u^*}{\Delta t} \eta_5 dx + \int_{I_j} \rho_h^n u_h^* \frac{\partial u_h^{n+1}}{\partial x} \eta_5 dx = -\nu \int_{I_j} q_h^{n+1} \eta_{5x} dx + \nu(\widehat{q}_h^{n+1} \eta_5^-)_{j+\frac{1}{2}} - \nu(\widehat{5}_h^{n+1} \eta_5^+)_{j-\frac{1}{2}}, \tag{27}$$

$$\int_{I_j} w_h^{n+1} \eta_6 dx + \int_{I_j} \chi_h^{n+1} \eta_{6x} dx - (\widehat{\chi}_h^{n+1} \eta_6^-)_{j+\frac{1}{2}} + (\widehat{\chi}_h^{n+1} \eta_6^+)_{j-\frac{1}{2}} = 0, \tag{28}$$

$$\int_{I_j} q_h^{n+1} \eta_7 dx + \int_{I_j} u_h^{n+1} \eta_{7x} dx - (\widehat{u}_h^{n+1} \eta_7^-)_{j+\frac{1}{2}} + (\widehat{u}_h^{n+1} \eta_7^+)_{j-\frac{1}{2}} = 0, \tag{29}$$

where r^{n+1} is updated by (25). The "hat terms in (22)–(29) in the cell boundary terms from integration by parts are the so called "numerical fluxes, which are single valued functions defined on the edges and should be designed based on different guiding principles for different PDEs to ensure stability. For the NSAC system with periodic boundary conditions, we choose the simple alternating numerical fluxes, such as

$$\begin{aligned}
&\hat{w}_h^{n+1} = w_h^{n+1+},\\
&\hat{\chi}_h^{n+1} = \chi_h^{n+1-},\\
&\hat{q}_h^{n+1} = q_h^{n+1+},\\
&\hat{u}_h^{n+1} = u_h^{n+1-}.
\end{aligned} \tag{30}$$

We remark that the choice for the fluxes (30) is not unique. Considering the compactness of the stencil and the optimal accuracy, the crucial part is taking $\hat{w}_h^{n+1}$ and $\hat{\chi}_h^{n+1}$ from opposite sides, $\hat{q}_h^{n+1}$ and $\hat{u}_h^{n+1}$ from opposite sides. With the definition of such numerical fluxes, it is easy to obtain that

$$-[w_h\chi_h]+\hat{w}_h[\chi_h]+\hat{\chi}_h[w_h]=0,$$
$$-[q_hu_h]+\hat{q}_h[u_h]+\hat{u}_h[q_h]=0,$$

where $[u_h]=u_h^+-u_h^-$ is the jump of the function u_h at each element boundary point. The distinctive feature of this minimal dissipation LDG method [22] is that the stabilization parameters associated with the numerical trace of the flux are identically equal to zero in the interior of the domain and the orders of convergence of the approximations for the potential and the flux using polynomials of degree k are the same as those of all known DG methods, namely, $(k+1)$ and k, respectively. Next, we will prove the linear and decoupled scheme is energy stable.

Theorem 3.1. *For the NSAC system (3a)–(3c) with periodic boundary condition for ρ, u and χ, the numeical solution to the LDG scheme (22)–(29) with the numerical fluxes (30) and the numerical fluxes*

$$\widehat{\rho_h^n u^*}=\rho_h^{n+}u^{*+} \text{ and } \widehat{G}_h^n=G(\rho_h^{n-}), \tag{31}$$

satisfies the energy stability

$$E_h(\rho_h^{n+1},u_h^{n+1},w_h^{n+1},r^{n+1})-E_h(\rho_h^n,u_h^n,w_h^n,r^n)\le 0, \tag{32}$$

where $E_h(\rho_h,u_h,w_h,r)=\frac{1}{2}\int_I\rho_hu_h^2dx+\frac{\epsilon}{2}\int_I w_h^2dx+\int_I\rho_hG(\rho_h)dx+\frac{1}{\epsilon}|r|^2$.

Proof. Taking the test function $\eta_1=u^*$ in (22), we derive that

$$\begin{aligned}&\frac{1}{2\Delta t}\int_{I_j}\rho_h^n\big((u^*)^2-(u_h^n)^2+(u^*-u_h^n)^2\big)dx-\int_{I_j}p_h^nu_x^*dx+(\widehat{p}_h^nu^{*-})_{j+\frac{1}{2}}-(\widehat{p}_h^nu^{*+})_{j-\frac{1}{2}}\\&=-\epsilon\int_{I_j}\frac{\partial w_h^{n+1}}{\partial x}w_h^nu^*dx.\end{aligned} \tag{33}$$

In (33), by the definition of $G(\rho)$ in (8), we have

$$-\int_{I_j}p_h^nu_x^*dx=-\int_{I_j}(\rho_h^nu^*)_x\big(\rho_h^nG'(\rho_h^n)+G(\rho_h^n)\big)dx+(\rho_h^{n-}u^{*-}\widehat{G})_{j+\frac{1}{2}}-(\rho_h^{n+}u^{*+}\widehat{G})_{j-\frac{1}{2}}. \tag{34}$$

Therefore, adding (33) and (26) with $\eta_4=\rho_h^nG'(\rho_h^n)+G(\rho_h^n)$, we obtain that

$$\begin{aligned}&\frac{1}{2\Delta t}\int_{I_j}\rho_h^n\big((u^*)^2-(u_h^n)^2+(u^*-u_h^n)^2\big)dx+\int_{I_j}\frac{\rho_h^{n+1}-\rho_h^n}{\Delta t}\big(\rho_h^nG'(\rho_h^n)+G(\rho_h^n)\big)dx\\&-\Big(\rho_h^{n-}u^{*-}\big(\rho_h^{n-}G'(\rho_h^{n-})+G(\rho_h^{n-})\big)\Big)_{j+\frac{1}{2}}+\Big(\rho_h^{n+}u^{*+}\big(\rho_h^{n+}G'(\rho_h^{n+})+G(\rho_h^{n+})\big)\Big)_{j-\frac{1}{2}}\\&+\Big(\widehat{\rho_h^nu^*}\big(\rho_h^{n-}G'(\rho_h^{n-})+G(\rho_h^{n-})\big)\Big)_{j+\frac{1}{2}}-\Big(\widehat{\rho_h^nu^*}\big(\rho_h^{n+}G'(\rho_h^{n+})+G(\rho_h^{n+})\big)\Big)_{j-\frac{1}{2}}\\&+\big((\rho_h^nu^*)^-\widehat{G}+\hat{p}_h^nu^{*-}\big)_{j+\frac{1}{2}}-\big((\rho_h^nu^*)^+\widehat{G}+\hat{p}_h^nu^{*+}\big)_{j-\frac{1}{2}}\\&=-\epsilon\int_{I_j}\frac{\partial w_h^{n+1}}{\partial x}w_h^nu^*dx,\end{aligned} \tag{35}$$

where

$$\hat{p}_h^n=(\widehat{\rho}_h^n)^2G'(\widehat{\rho}_h^n). \tag{36}$$

For (23), (24) and (28), we take the test functions as

$$\eta_2=\mu_h^{n+1},\ \ \eta_3=-\frac{\chi_h^{n+1}-\chi_h^n}{\Delta t},\ \ \eta_6=\frac{\epsilon}{\Delta t}w_h^{n+1}, \tag{37}$$

and combine them with Eq. (35), we obtain that

$$\begin{aligned}&\frac{1}{2\Delta t}\int_{I_j}(\rho_h^n(u^*)^2-\rho_h^n(u_h^n)^2)dx+\int_{I_j}\frac{\rho_h^{n+1}-\rho_h^n}{\Delta t}\big(\rho_h^nG'(\rho_h^n)+G(\rho_h^n)\big)dx\\&-\Big(\rho_h^{n-}u^{*-}\big(\rho_h^{n-}G'(\rho_h^{n-})+G(\rho_h^{n-})\big)\Big)_{j+\frac{1}{2}}+\Big(\rho_h^{n+}u^{*+}\big(\rho_h^{n+}G'(\rho_h^{n+})+G(\rho_h^{n+})\big)\Big)_{j-\frac{1}{2}}\\&+\Big(\widehat{\rho_h^nu^*}\big(\rho_h^{n-}G'(\rho_h^{n-})+G(\rho_h^{n-})\big)\Big)_{j+\frac{1}{2}}-\Big(\widehat{\rho_h^nu^*}\big(\rho_h^{n+}G'(\rho_h^{n+})+G(\rho_h^{n+})\big)\Big)_{j-\frac{1}{2}}\\&+\big((\rho_h^nu^*)^-\widehat{G}+\hat{p}_h^nu^{*-}\big)_{j+\frac{1}{2}}-\big((\rho_h^nu^*)^+\widehat{G}+\hat{p}_h^nu^{*+}\big)_{j-\frac{1}{2}}\end{aligned}$$

$$
\begin{aligned}
&+\frac{1}{2\epsilon\sqrt{E_1(\chi_h^n)}}(r^{n+1}+r^n)\int_{I_j}\rho_h^n\frac{\partial f^n}{\partial\chi_h^n}\frac{\chi_h^{n+1}-\chi_h^n}{\Delta t}dx+\frac{r^{n+1}+r^n}{2\epsilon\sqrt{E_1(\chi_h^n)}}\int_{I_j}\rho_h^n\frac{\partial f^n}{\partial\chi_h^n}\frac{\partial\chi_h^n}{\partial x}u^*dx\\
&+\frac{\epsilon}{2\Delta t}\int_{I_j}\big((w_h^{n+1})^2-(w_h^n)^2\big)dx-\frac{\epsilon}{\Delta t}((\hat{\chi}_h^{n+1}-\hat{\chi}_h^n)w_h^{n+1-})_{j+\frac12}+\frac{\epsilon}{\Delta t}((\hat{\chi}_h^{n+1}-\hat{\chi}_h^n)w_h^{n+1+})_{j-\frac12}\\
&+\frac{\epsilon}{\Delta t}((\chi_h^{n+1-}-\chi_h^{n-})w_h^{n+1-})_{j+\frac12}-\frac{\epsilon}{\Delta t}((\chi_h^{n+1+}-\chi_h^{n+})w_h^{n+1+})_{j-\frac12}\\
&-\frac{\epsilon}{\Delta t}\big((\chi_h^{n+1-}-\chi_h^{n-})\hat{w}_h^{n+1}\big)_{j+\frac12}+\frac{\epsilon}{\Delta t}\big((\chi_h^{n+1+}-\chi_h^{n+})\hat{w}_h^{n+1}\big)_{j-\frac12}\\
&\le-\int_{I_j}(\mu_h^{n+1})^2dx.
\end{aligned}\tag{38}
$$

Taking the test function $\eta_5=u_h^{n+1}$ in (27), adding (27) and (26) with $\eta_4=\frac12(u_h^{n+1})^2$, we have

$$
\begin{aligned}
&\frac{1}{2\Delta t}\int_{I_j}\rho_h^n\big((u_h^{n+1})^2-(u^*)^2+(u_h^{n+1}-u^*)^2\big)dx\\
&+\frac{1}{2\Delta t}\int_{I_j}\frac{\rho_h^{n+1}-\rho_h^n}{\Delta t}(u_h^{n+1})^2dx+\frac12(\widehat{\rho_h^nu^*}(u_h^{n+1-})^2)_{j+\frac12}-\frac12(\widehat{\rho_h^nu^*}(u_h^{n+1+})^2))_{j-\frac12}\\
&+\frac12(\rho^{n-}u^{*-}(\hat{u}_h^{n+1})^2)_{j+\frac12}-\frac12(\rho^{n+}u^{*+}(\hat{u}_h^{n+1})^2)_{j-\frac12}-\frac12(\rho^{n-}u^{*-}(u_h^{n+1-})^2)_{j+\frac12}+\frac12(\rho^{n+}u^{*+}(u_h^{n+1+})^2)_{j-\frac12}\\
&=-\nu\int_{I_j}q_h^{n+1}\frac{\partial u_h^{n+1}}{\partial x}dx+\nu(\widehat{q}_h^{n+1}u_h^{n+1-})_{j+\frac12}-\nu(\widehat{q}_h^{n+1}u_h^{n+1+})_{j-\frac12}.
\end{aligned}\tag{39}
$$

Summing (39) with (29) for $\eta_7=\nu q_h^{n+1}$, we can get

$$
\begin{aligned}
&\frac{1}{2\Delta t}\int_{I_j}\rho^n\big((u_h^{n+1})^2-(u^*)^2+(u_h^{n+1}-u^*)^2\big)dx\\
&+\frac{1}{2\Delta t}\int_{I_j}\frac{\rho_h^{n+1}-\rho_h^n}{\Delta t}(u_h^{n+1})^2dx+\frac12(\widehat{\rho_h^nu^*}(u_h^{n+1-})^2)_{j+\frac12}-\frac12(\widehat{\rho_h^nu^*}(u_h^{n+1+})^2))_{j-\frac12}\\
&+\frac12(\rho^{n-}u^{*-}(\widehat{u_h^{n+1}})^2)_{j+\frac12}-\frac12(\rho^{n+}u^{*+}(\widehat{u_h^{n+1}})^2)_{j-\frac12}-\frac12(\rho^{n-}u^{*-}(u_h^{n+1-})^2)_{j+\frac12}+\frac12(\rho^{n+}u^{*+}(u_h^{n+1+})^2)_{j-\frac12}\\
&=-\nu\int_{I_j}(q_h^{n+1})^2dx+\nu(\widehat{q}_h^{n+1}u_h^{n+1-})_{j+\frac12}-\nu(\widehat{q}_h^{n+1}u_h^{n+1+})_{j-\frac12}+\nu(\widehat{u}_h^{n+1}q_h^{n+1-})_{j+\frac12}-\nu(\widehat{u}_h^{n+1}q_h^{n+1+})_{j-\frac12}\\
&-\nu(q_h^{n+1-}u_h^{n+1-})_{j+\frac12}+\nu(q_h^{n+1+}u_h^{n+1+})_{j-\frac12}.
\end{aligned}\tag{40}
$$

By Taylor expansion, there exist φ such that

$$
\rho^{n+1}G(\rho^{n+1})=\rho^nG^(\rho^n)+\big(\rho^nG'(\rho^n)+G(\rho^n)\big)(\rho^{n+1}-\rho^n)+\frac{(\varphi G(\varphi))''}{2}(\rho^{n+1}-\rho^n)^2,\tag{41}
$$

where $(\varphi G(\varphi))''\ge0$, which can be easily verified. Summing up (38) and (40), using (41), with the alternating numerical fluxes (30) and the numerical fluxes (31) for $\widehat{\rho_h^nu^*}$ and $\widehat{G}_h^n$, after summation over j and taking into account the periodic boundary condition, we obtain that

$$
\begin{aligned}
&\frac{1}{2\Delta t}\int_I\big(\rho_h^{n+1}(u_h^{n+1})^2-\rho_h^n(u_h^n)^2\big)dx+\frac{\epsilon}{2\Delta t}\int_I\big((w_h^{n+1})^2-(w_h^n)^2\big)dx\\
&+\frac{1}{\Delta t}\int_I(\rho_h^{n+1}G(\rho_h^{n+1})-\rho_h^nG(\rho_h^n))dx+\frac{1}{2\epsilon\sqrt{E_1(\chi_h^n)}}(r^{n+1}+r^n)\int_I\rho_h^n\frac{\partial f^n}{\partial\chi_h^n}\frac{\chi_h^{n+1}-\chi_h^n}{\Delta t}dx\\
&+\frac{r^{n+1}+r^n}{2\epsilon\sqrt{E_1(\chi_h^n)}}\int_I\rho_h^n\frac{\partial f^n}{\partial\chi_h^n}\frac{\partial\chi_h^n}{\partial x}u^*dx\le0.
\end{aligned}\tag{42}
$$

Multiply (25) by $\frac{1}{\epsilon}(r^{n+1}+r^n)$ and combine with (42), it is easy to obtain that

$$
\begin{aligned}
&\frac{1}{2\Delta t}\int_I\big(\rho_h^{n+1}(u_h^{n+1})^2-\rho_h^n(u_h^n)^2\big)dx+\frac{\epsilon}{2\Delta t}\int_I\big((w_h^{n+1})^2-(w_h^n)^2\big)dx\\
&+\frac{1}{\Delta t}\int_I(\rho_h^{n+1}G(\rho_h^{n+1})-\rho_h^nG(\rho_h^n))dx+\frac1\epsilon(|r^{n+1}|^2-|r^n|^2)\le0.
\end{aligned}\tag{43}
$$

□

Remark 3.1. For compressible NSAC system (3a)–(3c) with the homogeneous Neumann boundary condition for ρ, u and χ, the proposed scheme (22)–(29) is also unconditionally energy stable.

3.4. Semi-implicit SDC method

In order to achieve high order accuracy in time, we would like to use the semi-implicit spectral deferred correction (SDC) method for time discretization [29], which can be used in a large class of problems, especially for highly nonlinear ODEs without separating of stiff and non-stiff components, which is general and efficient.

We briefly recall the semi-implicit SDC method in Guo et al. [29]. Consider a more general class of problem of the form

$$\begin{aligned} u_t &= F(t, u(t), u(t)), t \in [0, T], \\ u(0) &= u_0, \end{aligned} \tag{44}$$

where $u_0, u(t) \in \mathbb{R}^n$ and $F : \mathbb{R} \times \mathbb{R}^n \times \mathbb{R}^n \to \mathbb{R}^n$. The dependence on the second argument of F is non-stiff, while the dependence on the third argument of F is stiff. The main idea of the method is that the variable $u(t)$ appearing as the second argument of F is treated explicitly, while $u(t)$ appearing as the third argument is treated implicitly.

The semi-implicit SDC method is driven iteratively by the chosen low order method (14). For convenience, the linear and decoupled scheme (14) can be written in the form

$$\begin{aligned} \chi^{n+1} &= \chi^n + \Delta t L_1(\rho^n, u^n, \chi^n, \chi^{n+1}), \\ \rho^{n+1} &= \rho^n + \Delta t L_2(\rho^n, u^n, \chi^n, \chi^{n+1}), \\ u^{n+1} &= u^n + \Delta t L_3(\rho^n, u^n, \chi^n, u^{n+1}, \chi^{n+1}). \end{aligned} \tag{45}$$

Suppose now the time interval $[0, T]$ is divided into M non-overlapping intervals by the partition $0 = t_0 < t_1 < \ldots < t_n < \ldots < t_M = T$. We shall describe below the semi-implicit SDC method which will be used to advance from t^n to t^{n+1}. Let $\Delta t_n = t_{n+1} - t_n$ and u_n denotes the numerical approximation of $u(t_n)$, with $u_0 = u(0)$. Divide the time interval $[t_n, t_{n+1}]$ into P subintervals by choosing the points $t_{n,m}$ for $m = 0, 1, \ldots, P$ such that $t_n = t_{n,0} < t_{n,1} < \ldots < t_{n,m} < \ldots < t_{n,P} = t_{n+1}$. Let $\Delta t_{n,m} = t_{n,m+1} - t_{n,m}$ and $u^k_{n,m}$ denotes the kth order approximation to $u(t_{n,m})$. To avoid the instability of approximation at equispaced nodes for high order accuracy, the points $\{t_{n,m}\}_{m=0}^P$ are chosen to be the Chebyshev Gauss–Lobatto nodes on $[t_n, t_{n+1}]$. We can also use Gauss nodes. Starting from u^n, ρ^n, χ^n, we give the algorithm to calculate u^{n+1}, ρ^{n+1}, χ^{n+1} in the following.

Compute the initial approximation

$u^1_{n,0} = u^n$, $\rho^1_{n,0} = \rho^n$ and $\chi^1_{n,0} = \chi^n$.

Use a first order semi-implicit scheme (45) to compute approximate solutions χ^1, u^1 and ρ^1 at the nodes $\{t_{n,m}\}_{m=1}^P$, i.e., For $m = 0, \ldots, P-1$

$$\begin{aligned} \chi^1_{n,m+1} &= \chi^1_{n,m} + \Delta t_{n,m} L_1(\rho^1_{n,m}, u^1_{n,m}, \chi^1_{n,m}, \chi^1_{n,m+1}), \\ \rho^1_{n,m+1} &= \rho^1_{n,m} + \Delta t_{n,m} L_2(\rho^1_{n,m}, u^1_{n,m}, \chi^1_{n,m}, \chi^1_{n,m+1}), \\ u^1_{n,m+1} &= u^1_{n,m} + \Delta t_{n,m} L_3(\rho^1_{n,m}, u^1_{n,m}, \chi^1_{n,m}, u^1_{n,m+1}, \chi^1_{n,m+1}). \end{aligned} \tag{46}$$

Compute successive corrections

For $k = 1, \ldots, K$

$$u^{k+1}_{n,0} = u^n, \ \rho^{k+1}_{n,0} = \rho^n, \ \chi^{k+1}_{n,0} = \chi^n. \tag{47}$$

For $m = 0, \ldots, P-1$

$$\begin{aligned} \chi^{k+1}_{n,m+1} &= \chi^{k+1}_{n,m} + \Delta t_{n,m}\big(L_1(\rho^k_{n,m+1}, u^k_{n,m+1}, \chi^k_{n,m+1}, \chi^{k+1}_{n,m+1}) \\ &\quad - L_1(\rho^k_{n,m+1}, u^k_{n,m+1}, \chi^k_{n,m+1}, \chi^k_{n,m+1})\big) + I^{m+1}_m\big(L_1(\rho^k, u^k, \chi^k, \chi^k)\big), \\ \rho^{k+1}_{n,m+1} &= \rho^{k+1}_{n,m} + \Delta t_{n,m} L_2(\rho^{k+1}_{n,m}, u^{k+1}_{n,m}, \chi^{k+1}_{n,m}, \chi^{k+1}_{n,m+1}), \\ u^{k+1}_{n,m+1} &= u^{k+1}_{n,m} + \Delta t_{n,m}\big(L_3(\rho^k_{n,m+1}, u^k_{n,m+1}, \chi^k_{n,m+1}, u^{k+1}_{n,m+1}, \chi^{k+1}_{n,m+1}) \\ &\quad - L_3(\rho^k_{n,m+1}, u^k_{n,m+1}, \chi^k_{n,m+1}, u^k_{n,m+1}, \chi^k_{n,m+1})\big) + I^{m+1}_m\big(L_3(\rho^k, u^k, \chi^k, u^k, \chi^k)\big), \end{aligned} \tag{48}$$

where $I^{m+1}_m\big(L_1(\rho^k, u^k, \chi^k, \chi^k)\big)$ is the integral of the Pth degree interpolating polynomial on the P+1 points $\big(t_{n,m}, L_1(\rho^k_{n,m}, u^k_{n,m}, \chi^k_{n,m}, \chi^k_{n,m})\big)_{m=0}^P$ over the subinterval $[t_{n,m}, t_{n,m+1}]$. We approximate $L_1(\rho^k, u^k, \chi^k, \chi^k)$ by its Lagrange interpolation polynomials based on the Gauss type points, which has been described in Guo et al. [29]. Finally, we have $u^{n+1} = u^{K+1}_{n,P}$, $\rho^{n+1} = \rho^{K+1}_{n,P}$ and $\chi^{n+1} = \chi^{K+1}_{n,P}$.

We denote the above time discretization scheme as SDC^K_P. The accuracy order for the SDC^K_P scheme is

$$O(\tau^{\min[K+1, P+1]}), \tag{49}$$

with $\tau = \max_{n,m} \Delta t_{n,m}$. This local truncation error has been proved in Guo et al. [29].

Remark 3.2. For spatial discretization, we use the LDG method which is presented in Section 3.3. It is shown that the linear scheme (14) with LDG method is unconditionally stable. Although, there is no proof of stability for the semi-implicit SDC with LDG method, the numerical results suggest that it is energy stable.

Table 1
The linear and decoupled scheme with the exact solution (50): accuracy test at time $T = 0.5$, $\Delta t = 0.1\Delta x$ and $\Delta x = 2\pi/N$, uniform grid with N meshes.

	N	L^2 error	Order	L^∞ error	Order
$\mathcal{P}^0$	16	1.85e−1	–	9.32e−2	–
	32	9.12e−2	1.02	4.57e−2	1.03
	64	4.48e−2	1.02	2.27e−2	1.01
	128	2.23e−2	1.01	1.13e−2	1.01

Table 2
The SDC_2^2 scheme with the exact solution (50): accuracy test at time $T = 0.5$, $\Delta t = 0.1\Delta x$ and $\Delta x = 2\pi/N$, uniform grid with N meshes.

	N	L^2 error	Order	L^∞ error	Order
$\mathcal{P}^0$	16	9.28e−2	–	3.86e−2	–
	32	4.53e−2	1.03	1.85e−2	1.06
	64	2.23e−2	1.02	9.13e−3	1.02
	128	1.12e−2	1.00	4.54e−3	1.01
$\mathcal{P}^1$	16	2.12e−2	–	1.09e−2	–
	32	5.25e−3	2.01	2.58e−3	2.07
	64	1.31e−3	2.01	6.34e−4	2.02
	128	3.26e−4	2.00	1.61e−4	1.98
$\mathcal{P}^2$	16	2.65e−3	–	2.78e−3	–
	32	3.45e−4	2.94	3.54e−4	2.97
	64	4.45e−5	2.95	4.48e−5	2.98
	128	5.59e−6	2.99	5.62e−6	2.99

4. Numerical experiments

In this section, we present several numerical examples for the NSAC system. We use the LDG spatial discretization coupled with the energy stable scheme to study the large time behaviors of solutions to the initial value problems. We first present accuracy tests, which show the expected accuracy in both space and time with the proposed method. In our numerical experiments, the numerical fluxes (30) and (31) are used. Uniform grids are used in both 1D and 2D cases.

4.1. Accuracy and stability tests

Consider the NSAC system (3a)–(3c) in one dimensional domain $I = (-\pi, \pi)$ with periodic boundary condition. To verify the convergence rate, we choose the suitable forcing functions so that the exact solution is given by

$$\chi(x,t) = e^{-2t}\cos(x), \tag{50}$$

where $\epsilon = 1.0$ $\nu = 0.1$ and $\Theta = 1.5$. We use the LDG method for spatial discretization on the uniform mesh with mesh size $\Delta x = 2\pi/N$. The L^2 and L^∞ errors between exact solution and numerical solution, which are defined as

$$\| e \|_2 = \left(\sum_j \Delta x |e_j|^2 \right)^{1/2} \quad \text{and} \quad \| e \|_\infty = \max_j \{|e_j|\},$$

and the numerical order of accuracy at time $T = 0.5$ for the linear decoupled scheme are presented in Table 1, which indeed show the corresponding accuracy. Although the scheme is shown to be energy stable, the time step is still limited by the requirement that the truncation error must stay small and we take $\Delta t = 0.1\Delta x$ in all the spatial accuracy tests. In Table 1, the method (22)–(29) is used, which is first order in time, so we just consider $\mathcal{P}^0$ approximation.

To show that the proposed SDC method with LDG spatial discretization is high order accurate in both space and time, we choose $\mathcal{P}^\gamma, \gamma = 0, 1, 2$, approximation for spatial discretization and the SDC_P^K time marching method with $K = 2, P = 2$. Table 2 shows the L^2 and L^∞ errors and numerical orders of accuracy at time $T = 0.5$. We can see that the method with $\mathcal{P}^\gamma$ approximation gives a $(\gamma + 1)$th order of accuracy. To test the temporal accuracy of the accuracy of the SDC method, we choose $\mathcal{P}^4$ approximation and $N = 128$ to ensure that the spatial discretization error is small enough, such that the temporal discretization error is dominant. We present the L^2 and L^∞ errors and the numerical orders of temporal accuracy in Table 3, which shows the expected accuracy of the SDC method. Since at each time step, we solve the equations by an algebraic multigrid solver, the multigrid convergence rate is independent of Δx, where the multigrid smoothing sweep technique is Gauss–Seidel iteration and the number of pre/post-relaxations is fixed as 4 and the tolerance for the stopping criterion is 10^{-8}, which is also demonstrated in Guo and Xu [16]. For the same precision, the computational cost of the proposed

Table 3
Temporal accuracy test with the exact solution (50): accuracy test at time $T = 0.5$, $\Delta x = 2\pi/128$ and piecewise $\mathcal{P}^4$ approximations. The refinement path is $\Delta t = \Delta t_0/2^m$, $m = 0, 1, 2, 3$ and $\Delta t_0 = 0.025$.

	m	L^2 error	Order	L^∞ error	Order
SDC_2^0	0	1.21e−2	–	8.75e−3	–
	1	6.38e−3	0.92	4.61e−3	0.92
	2	3.25e−3	0.97	2.33e−3	0.98
	3	1.64e−3	0.99	1.17e−3	0.99
SDC_2^1	0	3.12e−3	–	1.02e−3	–
	1	8.23e−4	1.92	2.68e−4	1.92
	2	2.13e−4	1.95	6.98e−5	1.94
	3	5.36e−5	1.99	1.76e−5	1.98
SDC_2^2	0	3.25e−5	–	1.78e−5	–
	1	4.94e−6	2.71	2.58e−6	2.78
	2	6.86e−7	2.85	3.64e−7	2.82
	3	8.82e−8	2.96	4.83e−8	2.91

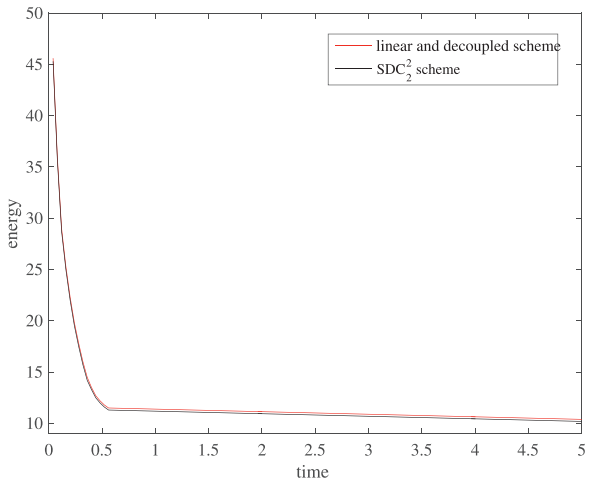

Fig. 1. The discrete energies using the linear and decoupled scheme, and the SDC scheme.

approach is less than the method in He and Shi [17], which presented a relaxation scheme coupled with a stabilized method to numerically study the compressible two–phase flow.

To test the energy stability, we use linear scheme (22)–(29), the SDC_2^2 time marching method with $\Delta t = 0.1\Delta x$ and advance the evolution to $T = 5.0$. The discrete energy is defined in (32), and we compute $G(\rho)$ by numerical quadrature. The traces of energy are presented in Fig. 1. We can see the energy using the linear and decoupled scheme is non-increasing in time, which agrees with the theoretical result. And for the SDC method driven by the first order linear scheme, the energy is also non-increasing, namely, it is stable numerically.

To further investigate the accuracy of the proposed method, we consider the NSAC system (52) in the two dimensional domain $\Omega = (-\pi, \pi) \times (-\pi, \pi)$ with periodic boundary condition. We choose the suitable forcing terms so that the exact solution is given by

$$\chi(x, y, t) = e^{-2t}\cos(x)\cos(y), \tag{51}$$

with the same values of ϵ, ν and Θ as in one dimensional case. The LDG method for spatial discretization is used on the uniform mesh with the mesh size $\Delta x = \Delta y = 2\pi/N$. Similar as in one dimensional case, we choose $\mathcal{P}^\gamma$, $\gamma = 0, 1, 2$, approximations for spatial discretization and the SDC_2^2 method for the temporal discretization. Table 4 presents the L^2 and L^∞ errors and the numerical orders of accuracy at time $T = 0.5$, which shows $(\gamma + 1)$th order of accuracy for $\mathcal{P}^\gamma$ approximation.

4.2. One dimensional cases

In order to investigate the phase separation dependence on initial data, we need to simulate the long time behavior of compressible NSAC system. We use SDC_2^2 scheme combined with LDG method with different initial data. The computational domain is (0,1) and the p is defined in (7). We present following cases with $\epsilon = 10^{-3}$, $\nu = 0.01$ and $\Theta = 0.9$:

Table 4
The SDC_2^2 scheme with the exact solution (51): accuracy test at time $T = 0.5$, $\Delta t = 0.1\Delta x$ and $\Delta x = \Delta y = 2\pi/N$.

	N	L^2 error	Order	L^∞ error	Order
$\mathcal{P}^0$	16	1.34e−1	–	8.63e−2	–
	32	6.56e−2	1.03	4.22e−2	1.03
	64	3.24e−2	1.01	2.08e−2	1.02
	128	1.62e−2	1.00	1.03e−2	1.01
$\mathcal{P}^1$	16	8.33e−2	–	7.49e−2	–
	32	2.06e−2	2.01	1.82e−2	2.04
	64	5.14e−3	2.00	4.48e−3	2.02
	128	1.29e−3	1.99	1.13e−3	1.99
$\mathcal{P}^2$	16	8.96e−3	–	9.23e−3	–
	32	1.15e−3	2.96	1.18e−3	2.96
	64	1.45e−4	2.98	1.48e−4	2.99
	128	1.82e−5	2.99	1.86e−5	2.99

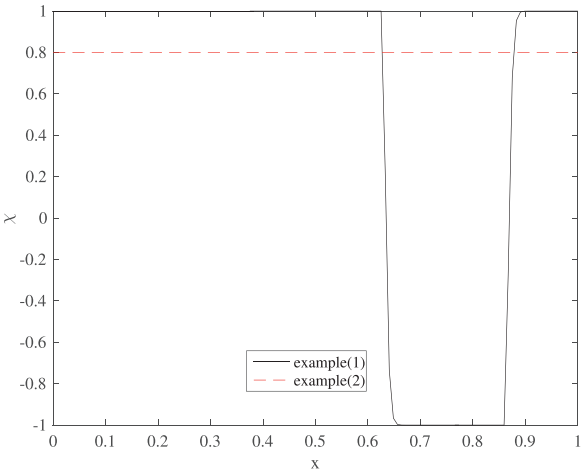

Fig. 2. Plot of χ at time $T = 10$.

(ex1) The initial data that lie in the unstable region with

$$(\rho_0, u_0, \chi_0)^T = \left(0.9 + 0.1\cos(2\pi x), 0.1e^{-5(x-0.5)^2}, 0.3 + 0.4\sin(2\pi x)\right)^T.$$

(ex2) The initial data that lie in the stable region with

$$(\rho_0, u_0, \chi_0)^T = \left(1.6 + 0.1\cos(2\pi x), 0.1e^{-5(x-0.5)^2}, 0.8 + 0.4\sin(2\pi x)\right)^T.$$

Periodic boundary condition is used in (ex1) and (ex2). Figs. 2–4 show the behaviors of χ, ρ and u at $T = 10$, when initial data is taken as (ex1) and (ex2). It is obvious to see that when the average of initial data is in an unstable region (ex1), the separation of phase is obtained in steady state. When the average of initial data is in a stable region (ex2), the solution remains in that region for all time. Both in these two examples, the discrete energy defined in (32) decays in time which shown in Fig. 5. The difference between (ex1) and (ex2) is the initial data of χ_0 and ρ_0, which is the essential reason that leads to the different asymptotical behaviors. The numerical simulations verify Theorem 3.1.

(ex3) The initial data is taken as

$$(\rho_0, u_0, \chi_0)^T = (1.0, 0.698, 0.3 + 0.4\sin(2\pi x))^T, \ 0 \geq x < 0.5,$$
$$(\rho_0, u_0, \chi_0)^T = (0.125, 0.0, 0.3 + 0.4\sin(2\pi x))^T, \ 0.5 \geq x \leq 1.0.$$

(ex4) The initial data is taken as

$$(\rho_0, u_0, \chi_0)^T = (0.8, 0.698, 0.7 + 0.3\sin(2\pi x))^T, \ 0 \geq x < 0.5,$$
$$(\rho_0, u_0, \chi_0)^T = (2.5, 0.0, 0.7 + 0.3\sin(2\pi x))^T, \ 0.5 \geq x \leq 1.0,$$

Figs. 6 –8 show the behaviors of χ, ρ and u at $T = 10$ when initial data is taken as (ex3) and (ex4). The average of initial data in (ex3) is in the unstable region, it is easy to observe the phase separation will greatly affect the evolution of density and velocity. The average of initial data in (ex4) is in the stable region, no phase separation will occur in the large time

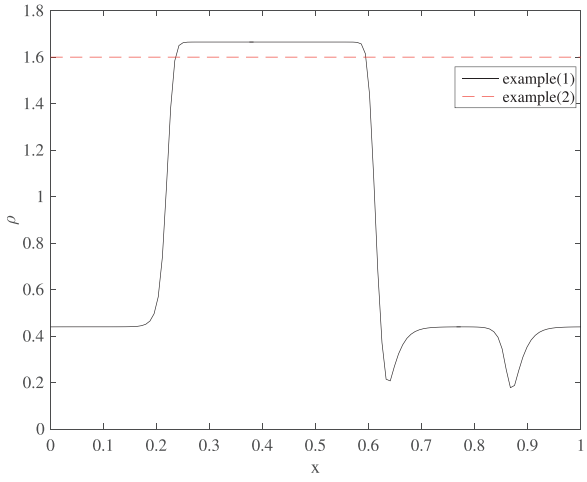

Fig. 3. Plot of ρ at time $T = 10$.

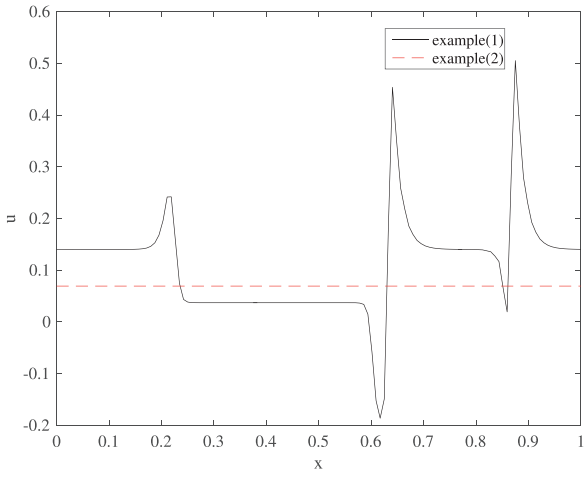

Fig. 4. Plot of u at time $T = 10$.

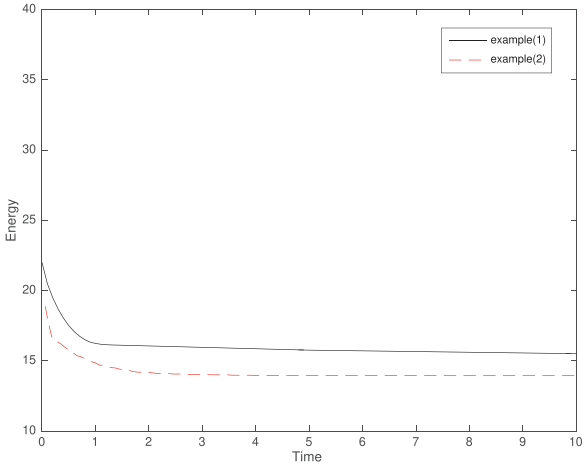

Fig. 5. Behavior of energy as a function of time.

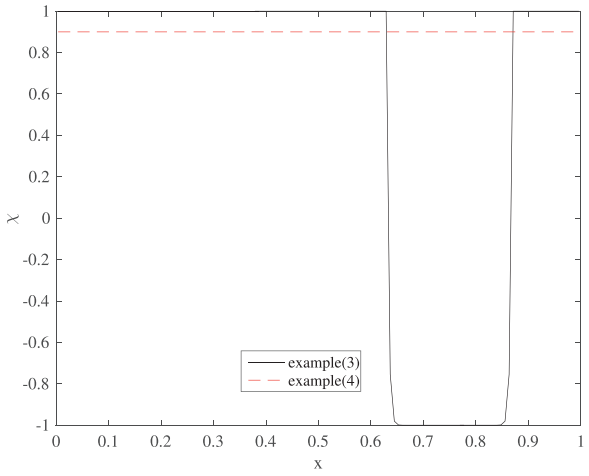

Fig. 6. Plot of χ at time $T = 10$.

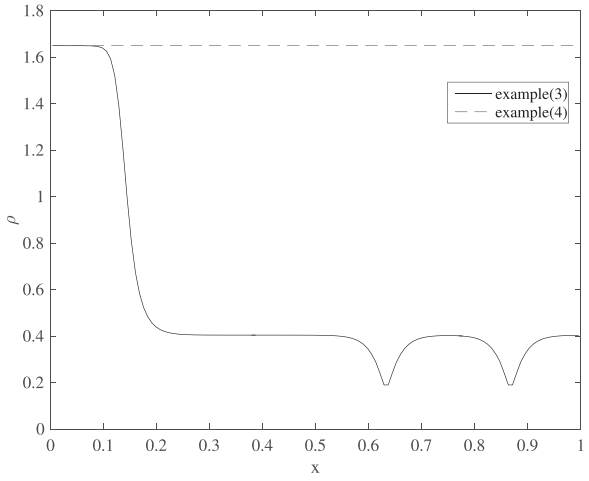

Fig. 7. Plot of ρ at time $T = 10$.

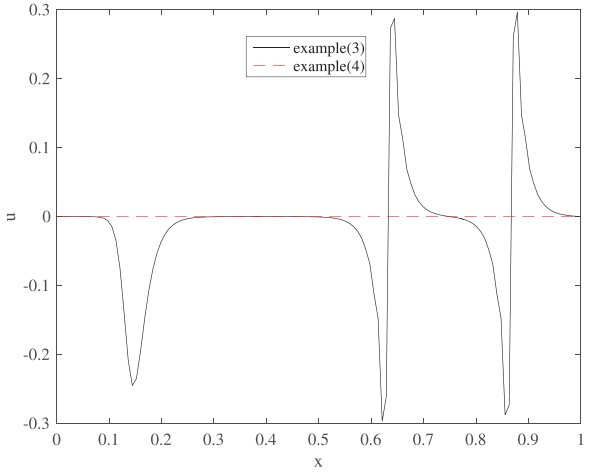

Fig. 8. Plot of u at time $T = 10$.

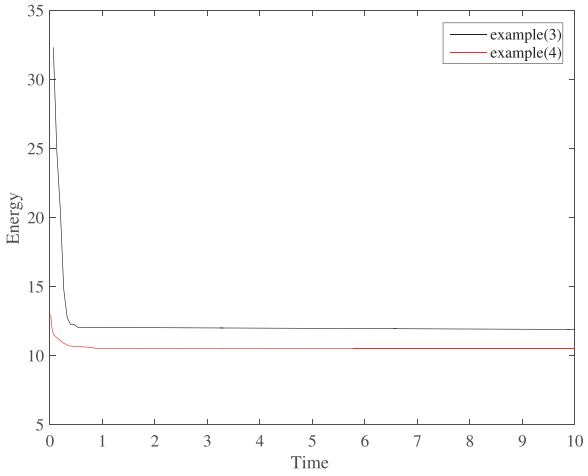

Fig. 9. Behavior of energy as a function of time.

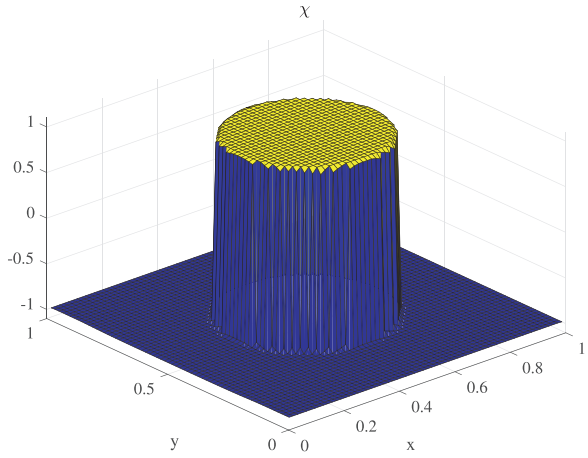

Fig. 10. Plot of χ at time $T = 10$.

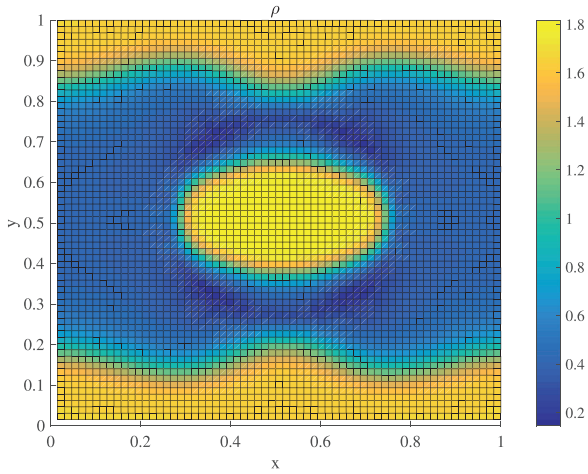

Fig. 11. Plot of ρ at time $T = 10$.

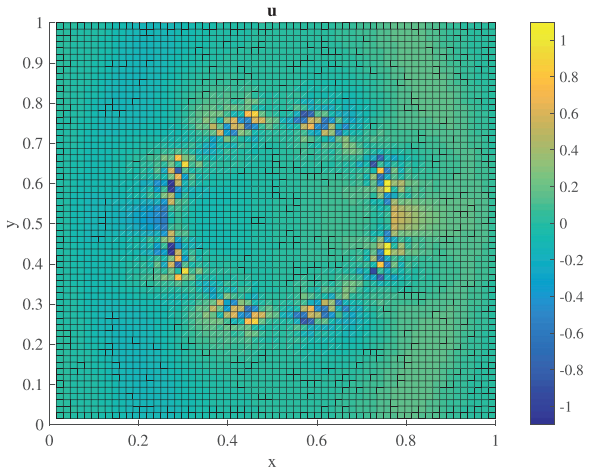

Fig. 12. Plot of horizontal velocity u at time $T = 10$.

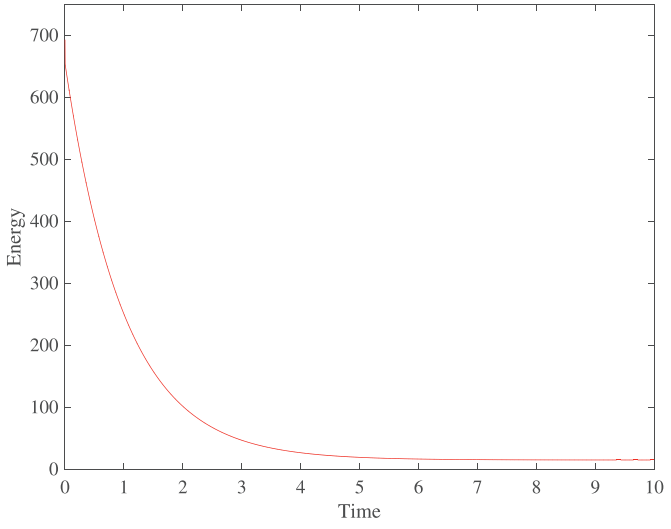

Fig. 13. Behavior of energy as a function of time.

behavior. Discrete energy decays in time which is shown in Fig. 9. The zero Neumann boundary condition is used in (ex3) and (ex4). Theorem 3.1 can be easily extended to such boundary condition.

4.3. Two dimensional cases

For two dimensional case, the compressible NSAC system is

$$\rho_t + (\rho u)_x + (\rho v)_y = 0,$$

$$(\rho u)_t + (\rho u^2 + p)_x + (\rho uv)_y = \nu \frac{2\partial u_x}{\partial x} + \nu \frac{\partial (u_y + v_x)}{\partial y} + \lambda \frac{\partial (u_x + v_y)}{\partial x}$$

$$-\epsilon \frac{\partial (\frac{1}{2}\chi_x^2 - \frac{1}{2}\chi_y^2)}{\partial x} - \epsilon \frac{\partial (\chi_x \chi_y)}{\partial y},$$

$$(\rho v)_t + (\rho uv)_x + (\rho v^2 + p)_y = \nu \frac{\partial (u_y + v_x)}{\partial x} + \nu \frac{2\partial v_y}{\partial y} + \lambda \frac{\partial (u_x + v_y)}{\partial y}$$

$$-\epsilon \frac{\partial (\chi_x \chi_y)}{\partial x} - \epsilon \frac{\partial (\frac{1}{2}\chi_y^2 - \frac{1}{2}\chi_x^2)}{\partial y},$$

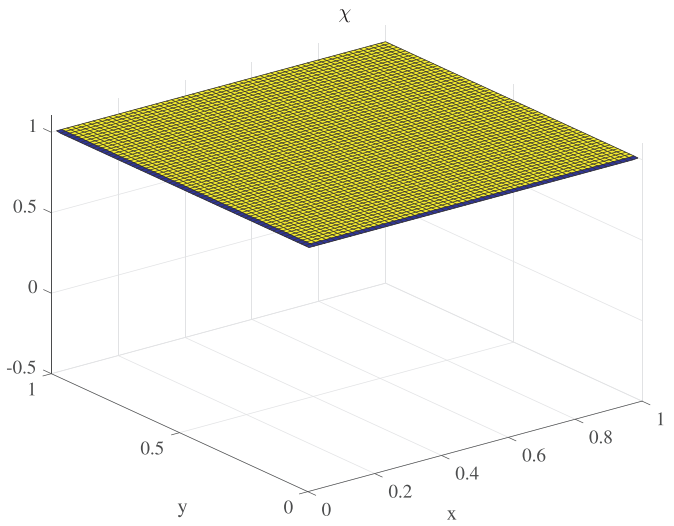

Fig. 14. Plot of χ at time $T = 10$.

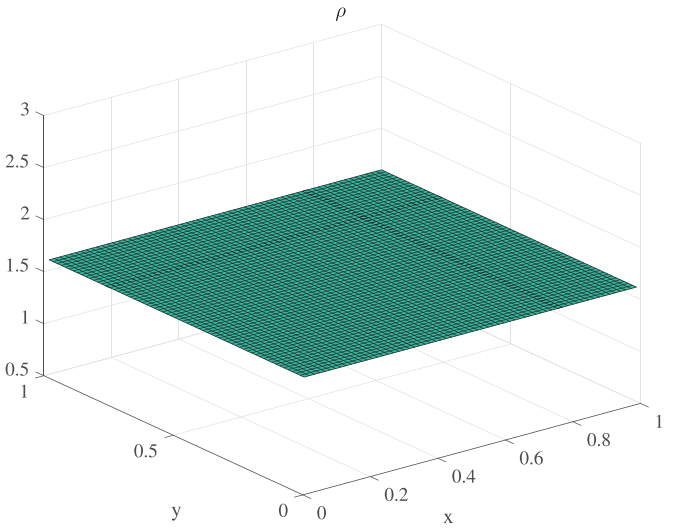

Fig. 15. Plot of ρ at time $T = 10$.

$$
\begin{aligned}
&(\rho\chi)_t + \frac{\partial(\rho\chi u)}{\partial x} + \frac{\partial(\rho\chi v)}{\partial y} = \mu,\\
&\rho\mu = \frac{1}{\epsilon}\rho\frac{\partial f(\chi)}{\partial \chi} - \epsilon \mathrm{div}(\nabla\chi),
\end{aligned} \tag{52}
$$

where the viscosity coefficients in (52) are $\lambda = 0.1$ and $\nu = 0.01$, the thickness $\epsilon = 10^{-3}$. The pressure is defined in (7) and $\Theta = 0.9$. The computational domain is $(0, 1) \times (0, 1)$. Periodic boundary condition is applied for ρ, u, v and χ both in x and y direction. For 2D case, the discrete energy is defined as $E_h = \frac{1}{2}\int_\Omega \rho_h(u_h^2 + v_h^2)dx + \frac{\epsilon}{2}\int_\Omega |\nabla\chi_h|^2 dx + \int_\Omega \rho_h G(\rho_h)dx + \frac{1}{\epsilon}|r|^2$. The initial data lie in the unstable region for (ex5). Figs. 10–12 show the separation of phase, and Fig. 13 shows that energy is decaying, which is similar to one dimensional case. The initial data lie in the stable region for example (ex6). Figs. 14–16 show the solutions go to a stable steady state, and Fig. 17 shows that energy is still decaying as predicted in Theorem 3.1.

(ex5) The initial data that lie in the unstable region with

$$
\begin{aligned}
(\rho_0, u_0, v_0, \chi_0)^T = \Big(&0.9 + 0.1\cos(2\pi x), 0.01e^{-5((x-0.5)^2+(y-0.5)^2)}, 0.01e^{-5((x-0.5)^2+(y-0.5)^2)},\\
&\tanh\left(\frac{-\sqrt{(x-0.5)^2+(y-0.5)^2}+0.25}{0.05}\right)\Big)^T,
\end{aligned}
$$

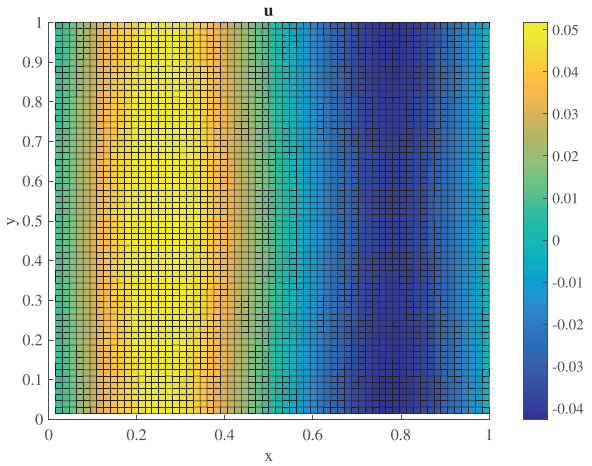

Fig. 16. Plot of horizontal velocity u at time $T = 10$.

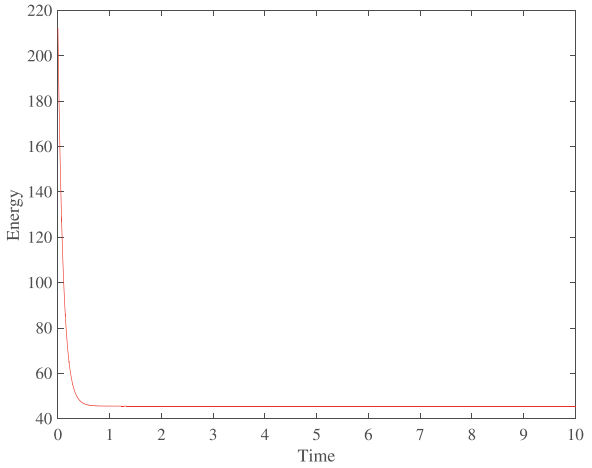

Fig. 17. Behavior of energy as a function of time.

(ex6) The initial data that lie in the stable region with

$$(\rho_0, u_0, v_0, \chi_0)^T = \Big(1.6 + 0.1\cos(2\pi x), 0.01e^{-5((x-0.5)^2+(y-0.5)^2)}, 0.01e^{-5((x-0.5)^2+(y-0.5)^2)}, \frac{1}{5.0}\tanh\left(\frac{-\sqrt{(x-0.5)^2+(y-0.5)^2}+0.25}{0.05}\right)+0.8\Big)^T.$$

5. Concluding remarks

We have presented a fully discrete LDG finite element method combined with SAV approach for the compressible NSAC system. It is worth to mention that the linear and decoupled scheme is easy to implement. The scheme is shown to have energy decaying property for one dimensional case which ensures stability of the scheme. Moreover, the semi-implicit SDC method combined with the linear and decoupled scheme is employed to improve the temporal accuracy. Numerical experiments have been presented to show that the combination of SDC method with LDG spatial discretization is indeed high order accurate in both time and space, and the method is energy stable numerically. Numerical results show that the initial state determines the long time behavior of the diffusive interface for the two–phase flow, phase separation or staying in stable region for all time, which verifies the asymptotic properties in Chen et al. [1] numerically.

Declaration of Competing Interest

The authors declare that they have no known competing financial interests or personal relationships that could have appeared to influence the work reported in this paper.

CRediT authorship contribution statement

Qiaolin He: Conceptualization, Methodology, Writing - original draft. **Xiaoding Shi:** Formal analysis, Investigation.

Acknowledgments

We thank Prof. Y. Xu for many useful discussions. This research is supported part by National Key R&D Program of China (2018YFC0830300) and the National Natural Science Foundation of China (Nos. 11671027, 11971020).

References

[1] Chen Y, He Q, Mei M, Shi X. Asymptotic stability of solutions for 1–D compressible Navier–Stokes–Cahn–Hilliard system. J Math Anal Appl 2018;467(1):185–206.
[2] Blesgen T. A generalization of the Navier–Stokes equations to two–phase flows. J Phys D 1999;32:1119–23.
[3] Feireis E, Petzeltová H, Rocca E, Schimperna G. Analysis of a phase–field model for two–phase compressible fluids. Math Models Methods Appl Sci 2010;20(7):1129–60.
[4] Heida M, Málek J, Rajagopal KR. On the development and generalizations of Allen–Cahn and Stefan equations within a thermodynamic framework. Z Angew Math Phys 2012;63(4):759–76.
[5] Ding S, Li Y, Luo W. Global solutions for a coupled compressible Navier–Stokes/Allen–Cahn system in 1D. J Math Fluid Mech 2013;15:335–60.
[6] Kotschote M. Strong solutions of the Navier–Stokes equations for a compressible fluid of Allen–Cahn type. Arch Ration Mech Anal 2012;206:489–514.
[7] Fermi E. Thermodynamics. Dover, New York; 1956.
[8] Sommerfeld A. Thermodynamics and statistical mechanics. Academic Press, New York and London; 1964.
[9] Affouf M, Caflisch R. A numerical study of Riemann problem solutions and stability for a system of viscous conservation laws of mixed type. SIAM J Appl Math 1991;51:605–34.
[10] Cockburn B, Gau H. A model numerical scheme for the propagation of phase transitions in solids. SIAM J Sci Comput 1996;17:1092–121.
[11] Slemrod M, Flaherty J. Numerical integration of a Riemann problem for a van der Waals fluids. Elias CA, John G, editors. New York: Elsevier; 1986.
[12] Hsieh D-Y, Wang X-P. Phase transition in van der Waals fluid. SIAM J Appl Math 1997;57:871–92.
[13] He Q, Liu C, Shi X. Numerical study of phase transition in van der Waals fluid. Discrete Contin Dyn Syst B 2018;23(10):4519–40.
[14] Gao M, Wang XP. A gradient stable scheme for a phase field model for the moving contact line problem. J Comput Phys 2012;231:1372–86.
[15] He Q, Glowinski R, Wang X-P. Numerical solution of the Navier–Stokes–Cahn–Hilliard system modeling the motion of the contact line. J Comput Phys 2011;230:4991–5009.
[16] Guo RH, Xu Y. Efficient, accurate and energy stable discontinuous Galerkin methods for phase field models of two–phase incompressible flows. Commun Comput Phys 2019;26(4):1224–48.
[17] He Q, Shi X. Numerical study of compressible Navier–Stokes–Cahn–Hilliard system. Commun Math Sci 2020;18(2):571–91.
[18] Shen J, Xu J, Yang X. The scalar auxiliary variable (SAV) approach for gradient flows. J Comput Phys 2018;353:407–16.
[19] Xu Y, Shu C-W. Local discontinuous Galerkin methods for high–order time-dependent partial differential equations. Commun Comput Phys 2010;7(1):1–46.
[20] Cockburn B, Shu C-W. The local discontinuous Galerkin method for time–dependent convection diffusion systems. SIAM J Numer Anal 1998;35:2440–63.
[21] Castillo P, Cockburn B, Perugia I, Schötzau D. An a priori error analysis of the local discontinuous Galerkin method for elliptic problems. SIAM J Numer Anal 2000;38(5):1676–706.
[22] Cockburn B, Dong B. An analysis of the minimal dissipation local discontinuous Galerkin method for convection–diffusion problems. J Sci Comput 2007;32(2):233–62.
[23] Guo R, Xu Y. Efficient solvers of discontinuous Galerkin discretization for the Cahn–Hilliard equations. J Sci Comput 2014;58:380–408.
[24] Guo R, Xia Y, Xu Y. An efficient fully–discrete local discontinuous Galerkin method for the Cahn–Hilliard–Hele–Shaw system. J Comput Phys 2014;264:23–40.
[25] Guo R, Xu Y. An efficient, unconditionally energy stable local discontinuous Galerkin scheme for the Cahn–Hilliard–Brinkman system. J Comput Phys 2015;298:387–405.
[26] Guo R, Xu Y, Xu Z. Local discontinuous Galerkin methods for the functionalized Cahn–Hilliard equation. J Sci Comput 2015;63:913–37.
[27] Guo R, Xu Y. Local discontinuous Galerkin method and high order semi-implicit scheme for the phase field crystal equation. SIAM J Sci Comput 2016;38:A105–27.
[28] Dutt A, Greengard L, Rikhlin V. Spectral deferred correction methods for ordinary differential equations. BIT Numer Math 2000;40:241–66.
[29] Guo R, Xia Y, Xu Y. Semi-implicit spectral deferred correction methods for highly nonlinear partial differential equations. J Comput Phys 2017;338:269–84.